5th Joint International Symposium on Deformation Monitoring (JISDM), 20-22 June 2022, Valencia, Spain
DOI: http://doi.org/10.4995/JISDM2022.2022.13830

Monitoring the production process of lightweight fibrous structures using terrestrial laser scanning

Laura Balangé[1, 2], Corinna Harmening[3], Rebeca Duque Estrada[4, 2], Achim Menges[4, 2], Hans Neuner[5], Volker Schwieger[1, 2]

[1] Institute of Engineering Geodesy, University of Stuttgart, Geschwister-Scholl-Str. 24D, 70174 Stuttgart, Germany, (laura.balange@iigs.uni-stuttgart.de; volker.schwieger@iigs.uni-stuttgart.de)
[2] Cluster of Excellence "Integrative Computational Design and Construction for Architecture", University of Stuttgart Keplerstraße 11, 70174 Stuttgart, Germany
[3] Geodetic Institute, Karlsruhe Institute of Technology, Englerstr. 7, 76131 Karlsruhe, Germany, (corinna.harmening@kit.edu)
[4] Institute for Computational Design and Construction, University of Stuttgart, Keplerstraße 11, 70174 Stuttgart, Germany, (rebeca.duque@icd.uni-stuttgart.de; achim.menges@icd.uni-stuttgart.de)
[5] Department of Geodesy and Geoinformation, Research Division Engineering Geodesy, TU Wien, Wiedner Hauptstraße 8, 1040 Vienna, Austria, (hans.neuner@geo.tuwien.ac.at)

Key words: *B-spline approximation; cross-sectional areas; laser scanning; lightweight fiber structures; monitoring; convex hull; quality assurance*

ABSTRACT

The Cluster of Excellence *Integrative Computational Design and Construction for Architecture* at the University of Stuttgart brings together various disciplines to jointly develop amongst other things a better understanding of processes in the manufacturing and construction domain. One of the cluster's aims is to create new solutions for the construction of lightweight fibrous structures using coreless winding of lightweight fiber composite systems. For this purpose, a precise geometry and an understanding of the fibers' behavior during the production process are of major importance. The fibers' production process is monitored by repeatedly scanning the fibers during different stages of the process using a terrestrial laser scanner. In order to determine the geometry of the fibers' axes as well as their cross-sections, two different strategies are used. The first strategy focuses on the segmentation of several straight lines between two intersection points. For the comparison of the individual fabrication steps, the positions of the intersection points are contrasted. For the cross-sectional areas of the fibers, orthogonal planes of intersection are then defined and all points within a predefined area are projected onto this plane. Then the area is calculated using a convex hull. In the second strategy, the fibers' main axes are represented by best-fitting B-spline curves. The borders of the cross-sections of interest are also approximated by best-fitting B-spline curves, forming the basis for the final determination of the cross-sectional areas. In this case study two epochs are analyzed with a deformation of the size of around 1cm. For both epochs the cross-sections are calculated in cm steps.

I. INTRODUCTION

Fiber-reinforced polymers (FRP) have been used for structural applications for many years in industries like automotive, aeronautics, and ship-building. Their wide application in these fields is due to a number of impressive properties, which in the case of carbon-fiber composites, include their low thermal expansion, high corrosion resistance, and their high strength to weight ratio (Fitzer, 1985).

Advances in robotic fabrication processes, such as coreless filament winding (CFW), enabled the manufacturing of highly differentiated FRP components, by relying the creation of a component on a designed sequence of fiber-fiber interaction instead of prefabricated winding mandrels or expensive formwork as commonly used in the industry (Prado *et. al.*, 2014). This fabrication technique has been developed and improved over the last decade at the University of Stuttgart through a series of projects and built demonstrators (Menges and Knippers, 2015; Prado *et al.*, 2017; Dambrosio *et al.*, 2019; Bodea *et al.*, 2021).

Such a fabrication system requires a high level of control over the fiber orientation since geometries are formed by the systematic sequence of fiber placement within a defined boundary condition. Geometrical differentiation is achieved through the combination of customized parameters, such as boundary geometry, winding pin locations, and sequence, also known as syntax. Their structural performance is directly dependent on good fiber-fiber interaction, that is when fibers are pressed against each other, ensuring that the system forms a lattice structure with reduced buckling length of each fiber segment (Prado *et al.,* 2014).

Predicting the interaction between fibers resulting from CFW is considered one of the biggest challenges during the design phase of such structures. As non-cured impregnated fibers do not possess any bending resistance during fabrication, every new fiber segment will deform the previously wound ones (Waimer *et al.,* 2013). The resulting deformation that induces the tension on the existing fibers will also be directly related to the final resulting form. This highly dynamic and incrementally changing system presents a challenge when being translated into a digital domain. A way to better inform and improve the simulation of CFW structures is by knowing more about what happens during the winding process. Understanding how different parameters can affect the consecutive deformations and final geometry can be helpful for fine-tuning the simulation method as well as for informing future design decisions.

The challenge from geodetic perspective is, that in contrast to conventional deformation analysis, the deformations are large compared to the object size (Dupuis *et al.*, 2016). For the cross-sections the challenge is, that they are very small compared to conventional applications like the cross-section of a tunnel or tree stem (Wang *et al.*, 2015; Eto *et al.*, 2020).

The aim of this contribution is to investigate the fiber geometry in each epoch. Therefore, the production process is monitored by repeatedly scanning different stages of the resulting fibers using terrestrial laser scanning. The parameters of interest, the position and orientation, describing the fibers' final geometry as well as the deformation between different production steps, the intersection between fibers and the area of fiber cross-sections are afterwards derived using two different strategies.

The paper is structured as follows: In Section II the mathematical basics that are required to derive the parameters of interest are provided. Section III presents details regarding the monitoring set-up. The two strategies used in this contribution to determine deformations and the final geometry are developed in Section IV. Section V presents, compares and discusses the results delivered by the two different strategies. Finally, Section VI concludes the paper.

II. Mathematical Basics

In this section, the mathematical basics of both algorithms are explained, which are needed to determine the position and orientation of the fibers as well as the area of the cross sections.

A. *Line Estimation*

The definition of a line is given by a direction vector as well as a base point. A main direction of a point cloud is in general given by the principal component analyses according to Pearson (1901). For the estimation of this direction the mean value of all points need to be calculated firstly. Afterwards the residuals of the point cloud are calculated by (Eq. 1):

$$\boldsymbol{\delta X} = \boldsymbol{X} - \boldsymbol{i} \cdot \boldsymbol{X}_{mean} \tag{1}$$

where $\boldsymbol{\delta X}$ = Residuals of the point cloud
$\boldsymbol{X}$ = Points of the point cloud
$\boldsymbol{i}$ = Matrix with ones with the dimension $n \times 3$
X_{mean} = Mean value of all points.

Using the residuals ordered as a line vector and the number of points the variance-covariance matrix is calculated by (Eq. 2):

$$\boldsymbol{C} = \frac{\boldsymbol{\delta X'} \cdot \boldsymbol{\delta X}}{n-1} \tag{2}$$

where $\boldsymbol{C}$ = variance-covariance matrix
$\boldsymbol{\delta X}$ = Residuals of the point cloud
n = Number of points.

A singular value decomposition of the variance-covariance matrix delivers the main direction of the point observations.

B. *Convex hull and area of polygon*

The convex hull of a planar data set is the minimum area convex polygon including all data points. For the estimation of the vertices of the convex hull several algorithms are established (Graham, 1972; Jarvis, 1973). In this investigation, the QuickHull algorithm was used (Green and Silvermann, 1979). Here, first the two points of the point set are determined with the minimum and maximum x coordinates, since these are certainly part of the convex hull. Then a line is drawn through both points and the set of points is divided into two halves by this line. Now the points with the maximum distance to the line in each point cloud half are searched for and a triangle is formed with it. All points within the triangle are not vertices of the convex hull. This is repeated with the two new triangle sides until all points are either a vertex of the convex hull or are within the convex hull.

With the vertices of the convex hull the area can be calculated by the equation calculated for convex polygons according to Bronstein *et. al.* (2001) as (Eq. 3):

$$A = \frac{1}{2}\sum_{j=1}^{k}\left(x_j y_{j+1} - x_{j+1} y_j\right) \tag{3}$$

where A = Area of the convex hull
x, y = Coordinates of the points
k = Number of points
j = point index, for $j = k$: $j + 1 = 1$

C. *Estimating best-fitting B-spline curves*

A B-spline curve $\boldsymbol{C}(u)$ is defined by Piegl and Tiller (1997) (Eq. 4):

$$\boldsymbol{C}(u) = \sum_{i=0}^{n_P} N_{i,p}(u) \cdot \boldsymbol{P}_i. \quad (4)$$

According to formula (Eq. 4), a three-dimensional curve point $\boldsymbol{C}(u) = [C_x(u) \quad C_y(u) \quad C_z(u)]^T$ is computed as the weighted average of the control points $\boldsymbol{P}_i$, with the weights being defined by the B-spline basis functions $N_{i,p}(u)$ of degree p. The basis functions can be computed recursively (Cox, 1972; de Boor, 1972) and are functions of the curve parameter *u,* locating a curve point on the curve. The corresponding parameter space $0 \leq u \leq 1$ is subdivided by means of a knot vector $\boldsymbol{U} = [u_0 \quad \dots \quad u_r]^T$, providing the B-spline's property of locality: The shifting of a single control point changes the curve only locally.

When using B-spline curves to approximate point clouds, the data points $\boldsymbol{C}(u)$ are the observations within a Gauss-Markov-Model (Bureick *et al.*, 2016) (Eq. 5):

$$\widehat{\boldsymbol{C}}(u) = \boldsymbol{C}(u) + \boldsymbol{\varepsilon} = f(\boldsymbol{P}_i), \quad (5)$$

where $\boldsymbol{\varepsilon}$ = residuals

Allowing for the estimation of the B-spline control points' positions. In order to obtain a linear estimation model, the remaining parameter groups (degree of the basis functions, knots, number of control points, curve parameters) are usually excluded from the estimation procedure and are determined in a different way. Choosing the optimal number of control points can be interpreted to be a model selection problem (Harmening and Neuner, 2016) and can be for example solved by classical model selection strategies e. g. BIC (Bayesian Information Criterion) or by means of structural risk minimization. If the latter strategy is used, the choice of the optimal degree of the basis functions can be included in the model selection task (Harmening, 2020). Sophisticated strategies for estimating the knot positions can be e. g. found in Bureick *et al.* (2019), whereas Piegl and Tiller (1997) propose a more simple, but also less computational complex method. For ordered data points standard strategies exist to allocate appropriate curve parameters to the observations (*cf. e. g*. Piegl and Tiller, 1997).

III. Monitoring Set-Up

For the test, a robotic fabrication setup was designed and implemented (*cf.* Figure 1). It was comprised of a 6-axis robotic arm coupled with a custom end-effector as well as a two-axis positioner and a reconfigurable frame. The material used was in the form of towpregs, which are pre-impregnated carbon fiber bundles pre-wound on spools. The spools were placed on the end-effector and the fiber was guided through rollers, eyelets, and a tube in order to be hooked around the anchors.

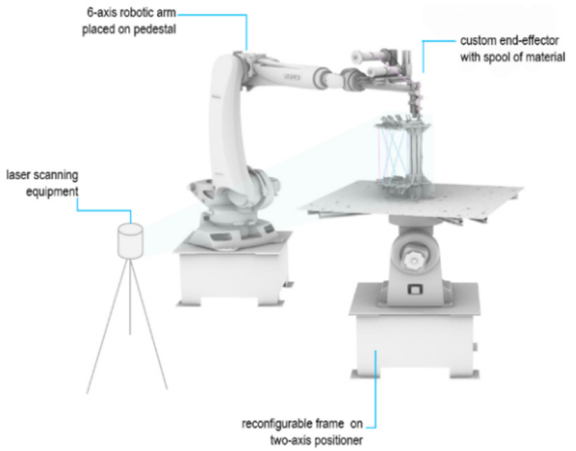

Figure 1. Robotic setup for coreless filament winding comprised of a 6-axis robotic arm coupled with an end-effector containing the spool of pre-impregnated carbon fibers, a two-axis positioner supporting the reconfigurable frame, and the laser scanning equipment.

All samples were fabricated with carbon fiber rovings pre-impregnated with epoxy resin. The fiber bundle was formed by two untwisted rovings with filament counts of 48 k and a 50-50 fiber/resin ratio. After being impregnated, the spools were stored in a cooling compartment in order to avoid the curing process to start. Before the beginning of fabrication, spools needed around 40 minutes to defrost. After reaching room temperature, the curing process starts, directly affecting the resin's viscosity. Even though fabrication time was kept to a minimum, it was still possible to observe different material behaviors related to the time the material was exposed to room temperature.

Considering the goal to understand how every new wound fiber could affect the whole system, the test required the scanning of the full fiber geometry after every new intersection was created.

In this study, measurements were taken with a Trimble X7 laser scanner. The measurements were carried out with a resolution of 5 mm at a distance of 10 m and a 3D point accuracy of 2.4 mm at 10 m (Trimble Inc., 2020). The elements have a height of approximately 40 cm and a width of 20 cm (*cf.* Figure 2) and a diameter of the fibers of 1 cm. The required accuracy for the measurements is in the range of several millimeters.

As part of the data pre-processing, a target based registration, as well as some filtering using the Statistical Outlier Removal (SOR) filter in CloudCompare was performed to detect and remove isolated points. For further data processing, the frame was also cut out and only the individual fibers were investigated. For the following investigations two measurement epochs

were considered. The measured epochs are visualized in Figure 3.

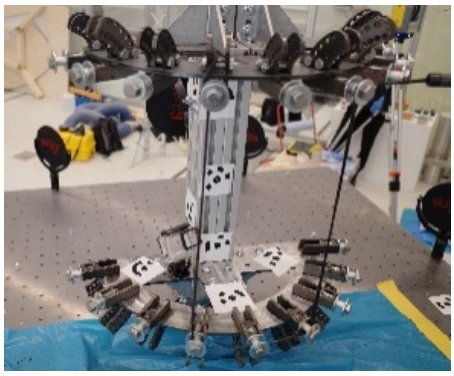

Figure 2. Monitoring set-up with the element in Epoch 1.

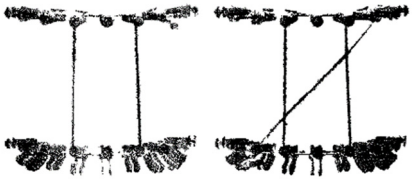

Figure 3. Measured Epochs. Left: first epoch with two separated fibers. Right: second epoch with one additionally crossed fiber.

The aim of this investigation is to determine the fiber geometry in each epoch. Here, the position and orientation of the fibers as well as the shape, namely the cross-sections, are taken into account.

IV. Determining the Shape of Lightweight Fibrous Structures

For the determination of the shape of the fiber two approaches were used. They are similar in their general procedure but differ in the specific calculation methods that are used. Figure 4 shows the workflow of both algorithms. The exact procedure is afterwards explained in the sections A and B.

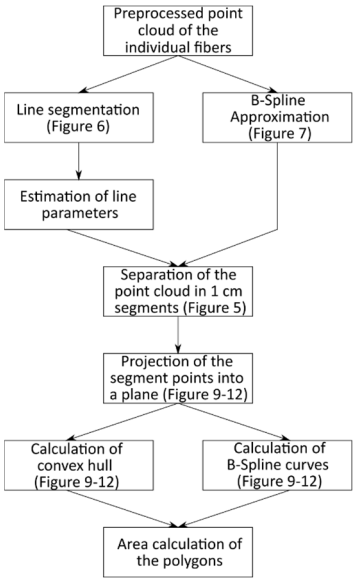

Figure 4. Workflow of the two approaches for shape detection of lightweight fibrous structures.

A. *Fiber approximation and area calculation using line segmentation and a convex hull*

In this approach, represented by the left side of Figure 4, the individual line segments are firstly segmented manually. A line estimation is then performed for the individual line segments. For this purpose, the direction of the straight line is determined by using a principal component analysis. In addition, the beginning and end of the segments are determined.

If the line parameter and the start and end point of all segments are available, the intersection points can be calculated. Therefore, all possible combinations between two segments are formed and the point of the minimal distance between the segments is calculated. To check whether the calculated point is an intersection point or not, firstly it is checked whether the point is within the volume of the point cloud. The second criteria for the decision is the distance to the segments. Here a limit of 5 mm has proven to be suitable in empirical tests. If all intersection points are found a clustering of these points needs to be done to find identical intersection points.

For this purpose, one of the selected intersection points is chosen randomly and the distances to all other points are calculated. All points with a distance less than 5 mm are combined into one intersection point. This value was chosen due to the fact, that in this case a distance between 5 mm between two intersections can be guaranteed. Among all assigned lines a common intersection point is determined. Since not all lines usually intersect at a single point, the sum of the distances of all lines to a common intersection point is minimized. This process is carried out iteratively until all intersection points are assigned.

In order to determine the deformation of the individual fibers between two epochs, the corresponding intersection point in the previous epoch must be determined. However, in the data set considered in this study, the intersection points in the first epoch do not yet exist. Therefore, to calculate the deformation, the minimum distance from the intersection point to all lines in the previous epoch is determined. The line with the minimum distance to the new intersection point is specified as the corresponding line. In addition, the perpendicular base point on this line is determined and the deformation can be calculated as the Euclidean distance between base point and intersection point.

In addition to the line parameters and intersections points, the cross-sectional areas of the individual line segments are also of importance. For this purpose, the line is firstly divided into 1 cm segments as shown in Figure 5.

The calculation of the cross-sectional areas takes place at these predefined positions. To calculate the area of a segment, a plane with the direction vector of the associated line is defined by the starting point of the segment on the line. Then a cylinder is created with the

direction vector of the estimated straight line as the axis of rotation with a radius of 15 mm around the segment. This limit was chosen, because it is larger than the actual radius of the fiber, but still small enough that no other fiber will be in the cylinder. Afterwards, all points that lie within the cylinder are determined and projected onto the previously created plane. For the calculation of the cross-sectional area, the convex hull is now formed around all projected points and then their surface area is calculated according to Equation (4).

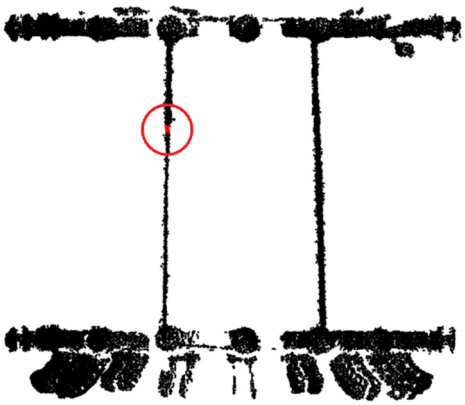

Figure 5. Point cloud of Epoch 1 (black) with one exemplary 1 cm segment (red).

B. *Fiber approximation and area calculation using B-spline curves*

The second strategy, represented by the right side of Figure 4, uses best-fitting B-spline curves to determine the shape of the fibers. For this purpose, point clouds representing a fiber are approximated by means of best fitting B-spline curves as described in Section II C. For all fibers cubic curves are chosen, with the optimal number of control points being determined by means of the Bayesian information criterion (Schwarz, 1978). The knot vectors are determined as proposed by Piegl and Tiller (1997) and the centripetal parameterization (*cf.* Piegl and Tiller, 1997) is chosen to allocate curve parameters to the observations. This strategy results in two B-spline curves for epoch 1 and three curves for epoch 2.

In analogy to approach A, the deformation of the fibers is represented by means of the behavior of two characteristic points. For this purpose, the intersection points of the fibers of the second epoch are determined: Therefore, the best-fitting B-spline curves are sampled with a very high resolution. Afterwards, for the curve representing the crossing fiber (*cf.* Figure 3), the nearest neighbors of the curve points representing the other two curves are determined. The results are two point pairs with minimal distance (for each pair, one point lies on the crossing fiber, the other point lies on one of the other two fibers). The final intersection points are then determined as the average of these point pairs. The correspondences of these points in the first measurement epoch are then defined by the nearest neighbors of these intersection points on the B-spline curves representing the fibers of the first measurement epoch.

The two characteristic points are complemented by means of the cross-sectional areas, completing the shape description of the fibers. To keep the determined cross-sectional areas comparable with the corresponding results delivered by strategy A, the same 1 cm-segments of the point clouds are used for the computations (see Figure 5).

In order to determine the cross-sectional areas, all points of the respective segment are initially projected in a plane by means of a principal component analysis. Afterwards, the boundary points of the projected segment are determined by means of the variant of the Douglas-Peucker-algorithm proposed in Harmening (2013). The detected boundary points provide the basis for the estimation of a closed B-spline curve, representing the segment's boundary. In principle, there exist three possibilities to obtain closed B-spline curves: The use of rational B-spline curves also allows for the representation of conic boundaries. However, in this application the number of observations is usually too small to jointly estimate control points and the corresponding weights. The second possibility is to stay with the non-rational B-splines and to close them by wrapping either the knots or the control points by means of constraints. This strategy also does not lead to satisfactory results due to the very few observations available. For this reason, the third and simplest approach is chosen: By selecting one of the boundary points as both the start and end points of the curve, a closed curve results.

Finally, the area surrounded by the B-spline curve is determined by interpreting the curve points of the sampled curve as a very fine polygon and by computing the area enclosed by this polygon.

V. Results

A. *Determination of the fibers' geometry and their deformation*

In the first part of the investigations, the fiber segments' geometry is determined by a segment-based line estimation as well as by means of a B-spline approximation. Both approximations of the point clouds are then used to determine characteristic points and to compute the deformation of these points.

Figure 6 graphically presents the results of the fibers' approximation by means of approach A (line approximation) in terms of the best fitting lines and the computed intersection points.

The results of approach B (B-spline fitting) are presented in Figure 7. Unlike approach A, in this approach the fibers are modeled as a whole and do not need to be further subdivided.

Finally, Table 1 contrasts the coordinates of the determined characteristic intersection points as well as the subsequently derived displacements of both

approaches. As can be seen, both the coordinates of the characteristic points as well as the deformation in terms of the absolute distance between these characteristic points are identical.

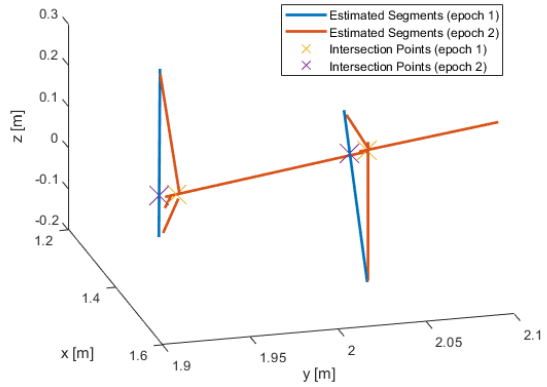

Figure 6. Results of line estimation and calculation of line intersection points.

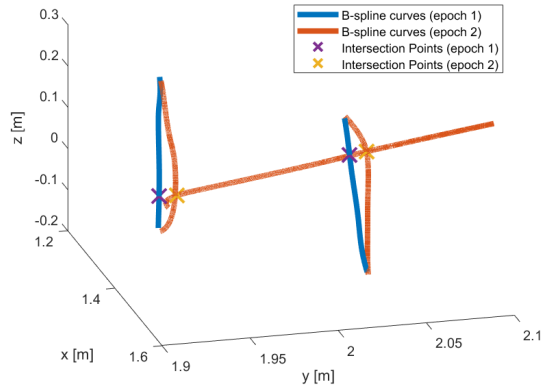

Figure 7. Results of the B-spline estimation and calculation of the respective intersection points.

Table 1. Intersection points and determined deformations

Intersection Point	Coordinates [m]			Deformation [m]
	X	Y	Z	
Point 1 (Line)	1.315	1.946	-0.051	0.010
Point 1 (B-Spline)	1.316	1.947	-0.051	0.010
Point 2 (Line)	1.498	2.030	0.152	0.012
Point 2 (B-Spline)	1.498	2.030	0.151	0.012

B. *Determination of the cross-sectional areas*

The results of the determination of the cross-sectional areas are summarized by means of Figure 8 as well as Table 2.

In Figure 8 the cross-sectional areas determined with the two described approaches are graphically opposed for the first measurement epoch as an example. Obviously, for most of the segments the B-spline-based approach determines the cross-sectional areas smaller than the approach based on the convex hull.

This result is supported by Table 2, summarizing the differences (Eq. 6)

$$d = \left||A_B - A_C|\right|, \quad (6)$$

where A_B = Cross-sectional areas delivered by the B- spline based approach
A_C = Cross-sectional areas delivered by the convex hull based approach

Of the determined cross-sectional areas by means of three parameters (mean value as well as minimum and maximum value).

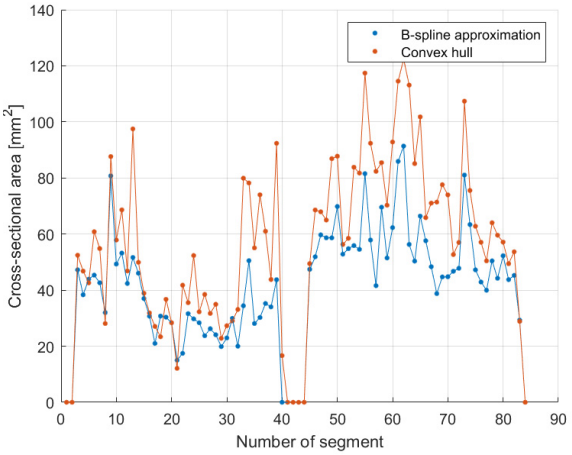

Figure 8. Cross-sectional areas of the first measurement epoch.

Table 2. Differences of the determined cross-sectional areas

	Epoch 1	Epoch 2
Mean(d) [mm²]	-16.21	-3.79
Min(d) [mm²]	-56.82	-70.80
Max(d) [mm²]	7.36	39.66

As can be seen, the mean values of the differences are negative in both epochs, underlining the fact that - on average - the B-spline-based approach delivers smaller cross-sectional areas than the approach based on the convex hull. However, this does not apply to all segments, as indicated by the maximum values of the differences, which are positive for both epochs. Hence, there do exist segments, for which approach A delivers smaller areas then approach B.

As furthermore indicated by the range of the differences, the magnitude of the differences varies strongly over the segments.

In order to investigate the causes of these deviations in more detail, the results of selected and representative individual segments are regarded. Figures 9 - 12 presents the results of four segments, which demonstrate the advantages and disadvantages of both approaches and, hence, allow for the explanation of the results in Figure 8 and Table 2. In all four figures the blue points represent the projected point cloud of the segment. The purple triangles are those points of the point cloud which define the convex hull (plotted in green), whereas the red crosses are the points detected to be boundary points that provide the

basis for the estimation of the surrounding B-spline curve (plotted in yellow).

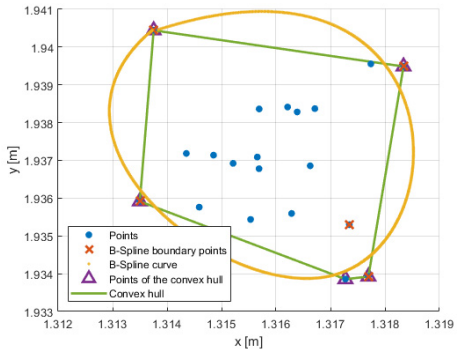

Figure 9. In detail investigation of the segments: Swinging out of the B-spline curve.

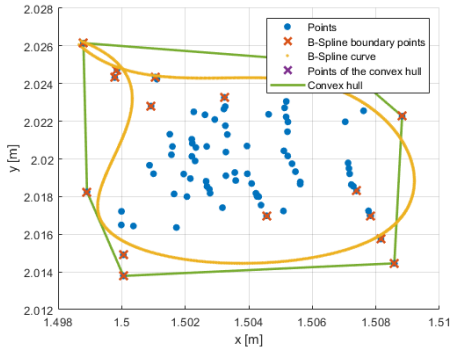

Figure 10. In detail investigation of the segments: Crossing over of the B-spline curve.

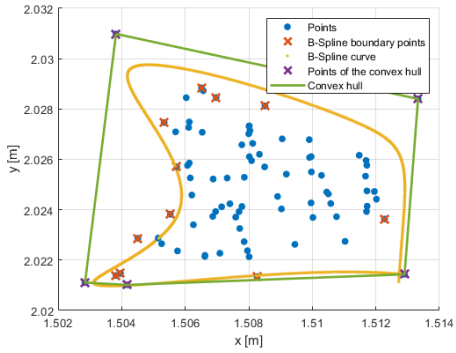

Figure 11. In detail investigation of the segments: Sensivity of the convex hull with respect to outliers.

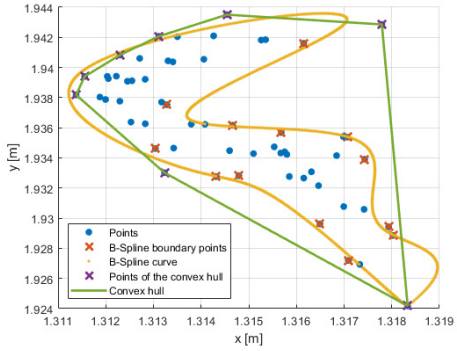

Figure 12. In detail investigation of the segments: Overestimation of the areas using the convex hull in case of complex and concave shaped boundaries.

In Figure 9 one of the rare situations, in which the B-spline-based approach results in a larger cross-sectional area than the convex hull-based approach, is presented. As can be seen, it is a segment with only few data points and, consequently, only few (six in this case) boundary points can be detected. With these six observations it is only possible to estimate a very simple B-spline curve, the shape of which is determined by less than six control points in order to maintain redundancy within the estimation problem (in the case presented four control points have been chosen). This simple B-spline curves swings off and does not any longer follow the actual boundary of the segment.

Figure 10 presents another weakness of the B-spline-based approach when only few boundary points can be detected. Due to the large gaps between the boundary points, the entire course of the curve is inadequately defined, allowing for the curve to cross over, a situation which is not desirable.

However, Figure 11 and Figure 12 present two situations in which the B-spline-based approach outperforms the convex-hull-based approach, pointing out the disadvantages of the latter as well the strengths of the former.

In both figures situations can be seen in which the cross-sectional areas determined by means of approach B are clearly smaller than those delivered by approach A. The reason for this becomes obvious when observing the point clouds: Apparently, some of the segments have concave boundaries, which cannot be approximated sufficiently well by means of a convex hull, resulting in overestimated cross-sectional areas.

Another reason for the convex-hull-based approach to overestimate the cross-sectional areas is its sensitivity with respect to outliers: The two upper purple triangles in Figure 11 do not seem to be part of the actual cross-section, rather it looks like they are outliers. However, being the boundary points of the segment, they define the convex-hull and, thus, the cross-section. These two points are also detected as boundary points within the B-spline-based approach. However, due to the redundancy within the estimation of the best-fitting B-spline curves, their influence on the curve's shape and, thus, on the cross-sectional area, is considerably smaller. As a consequence, the cross-sectional area delivered by approach B seems to be more realistic than the area resulting from approach A.

Finally, Figure 12 highlights another strength of the B-spline-based approach compared to the convex-hull-based approach: As indicated by the data points' distribution, some of the segments have very complex shapes. The flexibility of B-spline curves allows for the accurate modelling of these complex boundaries, whereas the use of the convex-hull does not.

Thus, the in detail investigation of the individual segments allows for the conclusion that approach A is the more appropriate method when the segments consist of only few data points and when the boundary is indeed convex. By contrast, the B-spline-based

approach delivers more satisfactory results when the boundaries are complex and/or concave shaped as well as when outliers exist.

VI. Conclusion

Within the framework of this project, the possibilities of two approaches were investigated in order to be able to realize a monitoring of the production process in the field of CFW and thus to be able to provide information about the interactions of the individual fibers during the production process. In addition, the shape of the fibers themselves, especially their cross-sectional area, was analyzed. In this study, point clouds from two measurement epochs were used to compare the two evaluation approaches. In the first approach a line estimation with subsequent calculation of the intersection points was carried out. In the second, the individual fibers were approximated by means of B-splines. In addition, the point cloud was separated in smaller segments with the size of 1 cm and the cross-section area was calculated with both approaches. Here approach one uses a convex hull and in approach two the area was calculated by the B-spline approach.

The comparison of the two approaches shows that both methods have their advantages as well as weaknesses and finally both methods achieve good results. For the calculation of the intersection points and thus also the path of the segments, both methods provide identical results and can therefore be considered equivalent. The calculation of the cross-sectional areas shows that the results of both methods strongly depend on the number and distribution of the measured points. The two methods were tested in this work on the basis of the same data, so that the uncertainties from the measurement process could be neglected for the comparison. An idea for the future is also to include some kind of outlier detection for the convex hull approach to improve the quality of the estimated area. A future improvement of the B-spline-based approach can be achieved by introducing constraints that prevent possible crossings of the curve. Furthermore, future research will include stochastic quantities to compare the results achieved by means of the two approaches. A necessary step for this are investigations regarding the stochastic properties of convex hulls.

However, in order to be able to make reliable statements about the geometry and shape of the fibers in the future, the quality of the used data set must be improved. Therefore, the material properties must also be taken into account. In addition to the specific properties of the resin, the fibers are moist during production and continue to dry over time. The investigation of these influences is therefore the focus of future work. This investigation is necessary as surface related uncertainties are of crucial importance for the final result (Chaudry, 2021). On idea for this is also the the use of a multi-color laser.

Another point that should be considered in future work is the possibility of automated segmentation of line segments, especially for larger and more complex elements. Also, the measurement configuration becomes more important, since the problem of covering individual fibers increases with the complexity.

VII. Acknowledgements

The research published in this article is supported by the Deutsche Forschungsgemeinschaft (DFG, German Research Foundation) under Germany's Excellence Strategy – EXC 2120/1 – 390831618. The authors cordially thank the DFG.

A part of the research was realized within a one-month research stay of the second author at the University of Stuttgart within the IntCDC incoming programme.

References

Bodea, S., C. Zechmeister, N. Dambrosio, M. Dörstelmann, and A. Menges (2021). *Robotic coreless filament winding for hyperboloid tubular composite components in construction. Automation in Construction, Elsevier*. DOI: 10.1016/j.autcon.2021.103649.

Bronstein, I. N., K. A. Semendjajew, G. Musiol, and H. Mühlig (2001). Taschenbuch der Mathematik. Edited by überarbeitete und erweiterte Auflage 5. Frankfurt am Main: Verlag Harri Deutsch.

Bureick, J., H. Alkhatib, and I. Neumann (2019). Fast converging elitist genetic algorithm for knot adjustment in B-spline curve approximation. *Journal of Applied Geodesy*. Vol. 13, Issue 4, pp. 317-328.

Bureick, J., H. Neuner, C. Harmening, and I. Neumann (2016). Curve and Surface Approximation of 3D Point Clouds. *Allgemeine Vermessungsnachrichten*, Vol. 123, Issue 11-12, pp. 315-327.

Chaudry, S. (2021). Surface related uncertainties of laser scanning: a simulation-based and experimental study. Dissertation. ETH Zürich, Zürich, Switzerland.

Cox, M.G. (1972). The Numerical Evaluation of B-Splines. *IMA Journal of Applied Mathematics*, Vol. 10, Issue 2, pp. 134-149.

de Boor, C. (1972). On calculating with B-splines. *Journal of Approximation Theory*, Vol. 6, Issue 1, pp. 50-62.

Dambrosio, N., C. Zechmeister, S. Bodea, V. Koslowski, M. Gil-Pérez, B. Rongen, J. Knippers, and A. Menges (2019). Towards an architectural application of novel fiber composite building systems – The BUGA Fibre Pavilion. *In ACADIA – Ubiquity and Autonomy [Proceedings of the ACADIA Conference 2019]*. The University of Texas, Austin. (ISBN 978-0-578-59179-7).

Dupuis, J., C. Holst, and H. Kuhlmann (2016). Laser scanning based growth analysis of plants as a new challenge for deformation monitoring. *Journal of Applied Geodesy*, Vol. 10, No. 1, 2016, pp. 37-44.

Eto, S., H.Masuda, Y Hiraoka, M. Matsushita, Michinari, M., and Takahashi, M. (2020). Precise Calculation Of Cross Sections And Volume For Tree Stem Using Point Clouds. *ISPRS - International Archives of the Photogrammetry, Remote Sensing and Spatial Information Sciences*. XLIII-B2-

2020. 205-210. DOI: 10.5194/isprs-archives-XLIII-B2-2020-205-2020.

Fitzer, E. (1985). Technical Status and Future Prospects of Carbon Fibres and their Application in Composites with Polymer Matrix (CFRPs). *Carbon Fibres and Their Composites*, 3–45. DOI:10.1007/978-3-642-70725-4_

Graham, R.L. (1972). An efficient algorithm for determining the convex hull of a finite planar set. *Information Processing Letters*, Vol 1, Issue 4, pp. 132-133.

Green, P.J., and B.W. Silvermann (1979). Constructing the convex hull of a set of points in the plane. *The Computer Journal,* Vol 22, Issue 3, pp. 262-266.

Harmening, C. (2013). Raum-zeitliche Segmentierung von natürlichen Objekten in stark verdeckten Szenen. Master thesis (unpublished). Leibniz University Hanover, Hanover, Germany.

Harmening, C. (2020). Spatio-temporal deformation analysis using enhanced B-spline models of laser scanning point clouds. Dissertation. TU Vienna, Vienna, Austria.

Harmening, C., and H. Neuner (2016). Choosing the Optimal Number of B-spline Control Points (Part 1: Methodology and Approximation of Curves). *Journal of Applied Geodesy*, Vol. 10, Issue 3, pp. 139-157.

Jarvis, R.A. (1973). On the identification of the convex hull of a finite set of points in the plane. *Information Processing Letters*, Vol 2, Issue 1, pp. 18-21.

Menges, A., and J. Knippers (2015). *Fibrous Tectonics*, *Architectural Design*, Vol. 85 No. 5, Wiley, London, pp. 40-47. ISBN 978-11118878378; DOI: 10.1002/ad.1952.

Pearson, K. F.R.S. (1901). LIII. On lines and planes of closest fit to systems of points in space. *The London, Edinburgh, and Dublin Philosophical Magazine and Journal of Science*, Vol. 2, Issue 11, pp. 559-572. DOI: 10.1080/14786440109462720.

Piegl, L., and W. Tiller (1997). The NURBS Book. Monographs in Visual Communication. Springer, Berlin and Heidelberg, 2nd edition.

Prado, M., M. Doerstelmann, J. Solly, A. Menges, and J. Knippers (2017). Elytra Filament Pavilion: Robotic Filament Winding for Structural Composite Building Systems. *In Fabricate – Rethinking Design and Construction [Proceedings of the Fabricate Conference 2017],* Stuttgart, pp. 224–233. (ISBN: 978 1 78735 001 4; JSTORE: j.ctt1n7qkg7.35).

Prado, M., M. Dörstelmann, T. Schwinn, A. Menges, and J. Knippers, (2014). Core-Less Filament Winding. DOI: 10.1007/978-3-319-04663-1_19.

Schwarz, G. (1978). Estimating the Dimension of a Model. *The Annals of Statistics*, Vol. 6, Issue 2, pp. 461-464.

Trimble Inc. (2020). Datasheet - Trimble X7. Available in: https://geospatial.trimble.com (accessed: 2021-12-10).

Waimer, F., R. La Magna, and J. Knippers (2013). Integrative Numerical Techniques for Fibre Reinforced Polymers - Forming Process and Analysis of Differentiated Anisotropy. *Journal of the International Association for Shell and Spatial Structures*. 54.

Wang, Z., Q. Lan, and E.Wang (2015). Automatically extracting contours of cross-sections from 3D point clouds of tunnel. *Proceedings of the International Conference on Advances in Mechanical Engineering and Industrial Informatics.* pp.8-15. DOI:10.2991/ameii-15.2015.2.